Local carbon emission zone construction in the highly urbanized regions: Application of residential and transport CO$_2$ emissions in Shanghai, China

Yunfeng Tian [a,b], Shudi Zuo [a,*], Jiaheng Ju [c], Shaoqing Dai [d], Yin Ren [a], Panfeng Dou [e]

[a] Key Laboratory of Urban Environment and Health, Fujian Key Laboratory of Watershed Ecology, Key Laboratory of Urban Metabolism of Xiamen, Institute of Urban Environment, Chinese Academy of Sciences, Xiamen, 361021, China
[b] University of Chinese Academy of Sciences, Beijing, 100049, China
[c] Department of Architecture and Built Environment, University of Nottingham Ningbo China, 315100, Ningbo, China
[d] Faculty of Geo-information Science and Earth Observation (ITC), University of Twente, Enschede, 7500AE, the Netherlands
[e] School of Civil Engineering, Putian University, Putian, 351100, China

ARTICLE INFO

ABSTRACT

Optimizing urban morphology can help city managers deploy internal carbon reduction strategies. However, due to the numerous factors that influence urban carbon emissions and the complex paths of their effects, existing research findings are diverse and difficult to compare. This study constructed the local carbon emission zone (LCEZ) which links the highly urbanization morphology profiles and CO$_2$ emission intensity to favor summarizing the form characteristics for the low CO$_2$ emission control in new communities. The approach involved selecting six indicators from the perspectives of urban external morphology, internal characteristics, and development intensity, and using geographically weighted regression (GWR) to identify three key factors. The selected factors were divided into low(1) medium(2) and high(3) categories and were combined with each other to construct the LCEZ. The nonparametric test and GeoDetector model were used to test the difference and similarity of LCEZs, respectively. The results showed that 1) The impacts of functional mixing entropy (FME), building height (BH) and road density (RD) on residential and transport CO$_2$ emissions (RTCE) were relatively large and positive; 2) The low- and medium-FME areas were the major types of LCEZ; 3) The area proportions of the low FME LCEZs in different population areas of the RTCE cold spot regions were the highest (81.84%–88.25%); 4) It is recommended that the morphological feature values of compact-low rise-low network (1-1-1), mid compact-low rise-mid network (1-1-2), compact-mid rise-low network (1-2-1) and mid compact-mid rise-mid network (1-2-2) were taken as the low CO$_2$ emission control of highly urbanized regions.

1. Introduction

By 2050, the population of urban residents will reach 66% of the global population. CO$_2$ emissions from energy use related to residents' living requirements will also increase significantly, eventually becoming the core part of urban CO$_2$ emissions [1]. Urban low-carbon technology is the inevitable choice of the current urban development path [2]. The adjustment of industrial structure and layout, energy saving, and utilization are the mainstream approaches to reduce urban CO$_2$ emissions including fossil fuel emissions (e.g. industry, transportation, and building sectors). Nevertheless, with the deepening of research, scholars have shifted their attentions to optimizing urban form features, which change residents' choices and behaviors, to generate less residential CO$_2$

emissions including building and transportation emissions [3]. Urban form features have impacted on the regional CO$_2$ emissions, change energy use patterns, and ultimately affect the rate and the amount of CO$_2$ emissions [4]. Studies had found that urban form can explain nearly half of urban residents' CO$_2$ emissions [5,6]. Although different urban types follow different urban form evolution paths, similar urban form patterns may result in similar spatial characteristics of CO$_2$ emissions in energy use. Therefore, defining a variety of urban form patterns and exploring the relationship between typical urban form patterns and CO$_2$ emission patterns can provide scientific guidance for the specific practice of low-carbon urban planning [7].

Urban physical form is the spatial allocation of human activities [8]. Urban form affects the residential CO$_2$ emissions through residents'

* Corresponding author. Institute of Urban Environment, Chinese Academy of Sciences 1799 Jimei Avenue, Xiamen, Fujian, China.
E-mail addresses: yftian@iue.ac.cn (Y. Tian), sdzuo@iue.ac.cn (S. Zuo), saxjj2@nottingham.edu.cn (J. Ju), s.dai@utwente.nl (S. Dai), yren@iue.ac.cn (Y. Ren), pfdou@ptu.edu.cn (P. Dou).

housing choice, travel characteristics, and surrounding thermal environment [8–11]. In recent years, the main research developed urban form characterization methods and models, explored the linear direct relationship between urban form (e.g. fragmentation, compactness, land use mixing) and CO_2 emission in different regions under various grid scales and time series, and analyzed the intermediary factors affecting residents' CO_2 emission. Some hypotheses of the working path were proposed [12–15]. Scholars classified the impact factors from various perspectives. Zuo et al. divided the form characteristics affecting CO_2 emissions into three aspects including external morphology, internal characteristics and development intensity [6]. Besides, Sharifi et al. built the estimation model between carbon emission and urban form from the perspective of building and transport network geometric properties and functional intensity, including building height, density, use, road network length, and configuration [16]. Zhang et al. divided them into urban pattern structure, functional organization type, and built environment in terms of 70 related articles published between 2005 and 2020 [17]. Urban pattern structure was the research content of spatial planning at the macro level. Functional organization type was the mid-level research content that focuses on the spatial planning of urban land resources. The built environment refers to the convenience facilities built and configured to meet the needs of human activities. However, except for the physical urban form factors, the socioeconomic factors, as a part of urban form, influenced the CO_2 emissions. Therefore, the division of external morphology, internal characteristics, and development intensity considering socioeconomic factors was comprehensive. The common indicators of external morphology can be divided into landscape metrics and indicators, which can be intuitively felt (e.g. height, sparse road network). The internal characteristics refer to the richness of different land use types from the perspective of urban functional organization types. Development intensity indicators are mainly morphological characteristics brought by the urban size effect and are carrier characteristics matching the development of economic activities, such as road density and building density.

There is no effective correlation between the research results and conclusions of the influence mechanism of urban form and the practical tools of urban planning [17]. The research results based on the administrative boundary of the whole city can only guide the overall strategic planning, and it is difficult to guide the practice in the detailed planning of specific regions. However, the emergence of spatial grid data on CO_2 emissions provides a basis for further research. Based on the typical morphological differences affecting urban CO_2 emissions, the key morphological index and their value ranges can be summarized based on the grid pixel as the analysis unit, which can effectively establish the relationship between research results and planning practice. Similar ideas have been applied in planning practice, such as Traffic Analysis Zone (TAZ) for rational distribution of traffic demand and Local Climate Zone (LCZ) for reducing the urban heat island effect. The zoning methods mainly include data-driven clustering and feature segmentation based on key influencing factors (building height and underlying surface type). TAZ is mostly based on data-driven clustering, which has the advantage of large inter-group differences and small intra-group differences. However, it requires large input data and is difficult to interpret typical features of grouped data. LCZ based on the characteristics of key factors is simple, but it is not suitable for the case of excessive key factors due to the exponential growth of the relationship between the number of key factors and the group type.

Urban form (e.g. configurations and land surface properties) affects microclimate, which in turn affects building energy use and CO_2 emissions. Many studies have analyzed the relationship between urban CO_2 emissions and urban form based on LCZ [18–20]. Cai et al. used the 54

landscape metrics at the class level and landscape level based on the 13 LCZ classed to represent the urban form [20]. There is the rare effective correlation between research conclusions and urban planning practice. In addition, studies have shown that the mixed degree of land use types and functions has an important impact on urban CO_2 emissions [21]. However, the LCZ does not consider such factors. Therefore, there is an obvious research gap at present. When using the LCZ partition method to analyze the relationship between urban morphology and CO_2 emissions, the impact of land use type and functional area mixing degree on urban CO_2 emissions is not considered. Therefore, based on the LCZ zoning, it is necessary to increase the key factors affecting urban CO_2 emissions such as the mixing degree of functional areas, and construct the local carbon emission zone (LCEZ) representing different typical cities to improve the accuracy of the results of the analysis of the impact of urban form on CO_2 emissions. At the same time, it connects the research results with the planning practice application. To address the research gaps mentioned above, we selected the highly urbanized region to control the influences of the urban aggregation effect and developed a LCEZ construction framework concerning the local spatial heterogeneity. The framework identified the key factors, which were combined to form the LCEZ, affecting urban CO_2 emissions in different urbanization gradients and climate zones. There were three steps of the proposed method. Firstly, we mapped the CO_2 emission at the grid scale. Secondly, we identified the key factors affecting urban CO_2 emissions and then combined key factors to form different LCEZ. The basic assumption is that the surface and urban morphological characteristics are similar in the same LCEZ. Thirdly, the form characteristics of LCEZs in the low-low aggregation region of the residential CO_2 emission were analyzed. The results favored the connection of the mesoscale and micro-scale planning information. This study intended to: 1) map the spatial distribution of residential transport CO_2 emissions (RTCE) which was suitable for urban scale analysis. Based on the statistical yearbook and traffic data, we integrated multi-source data through the downscaling and bottom-up methods to map RTCE in the core region. 2) To screen urban form factors affecting RTCEs to construct the LCEZ. From the three aspects of external morphology, internal characteristic, and development intensity, geographically weighted regression (GWR) was used to screen the key factors affecting residential energy use. A parameter system was constructed to define LCEZ. Non-parametric test and Geographical detector model were used to verify the differences and similarities of LCEZ, respectively. 3) To apply the LCEZ construction method in the new communities. The representative urban form types and features with low CO_2 emission intensity, which could be used in the new communities, were detected in the core region of Shanghai.

2. Materials and methods

2.1. Study area

Shanghai is the core city of the Yangtze River Delta in China. There are 16 municipal districts with a total area of 6,340.5 km². The rapid economic development has accelerated the urbanization process of Shanghai. In 2019, the GDP of Shanghai was 3,815.532 billion yuan. The population was 24.81 million. The high population density resulted in the high urbanization rate (88.10%), which was the highest in China. The urbanization leads to great changes in land use and the physical properties of the underlying surface. The surface temperature in the northern central city of Shanghai is higher than that in other areas during the daytime, forming a strong urban heat island effect [22].

This study selected the core urban area as the research area. According to the Global Urban Boundary (GUB) dataset [23], we defined
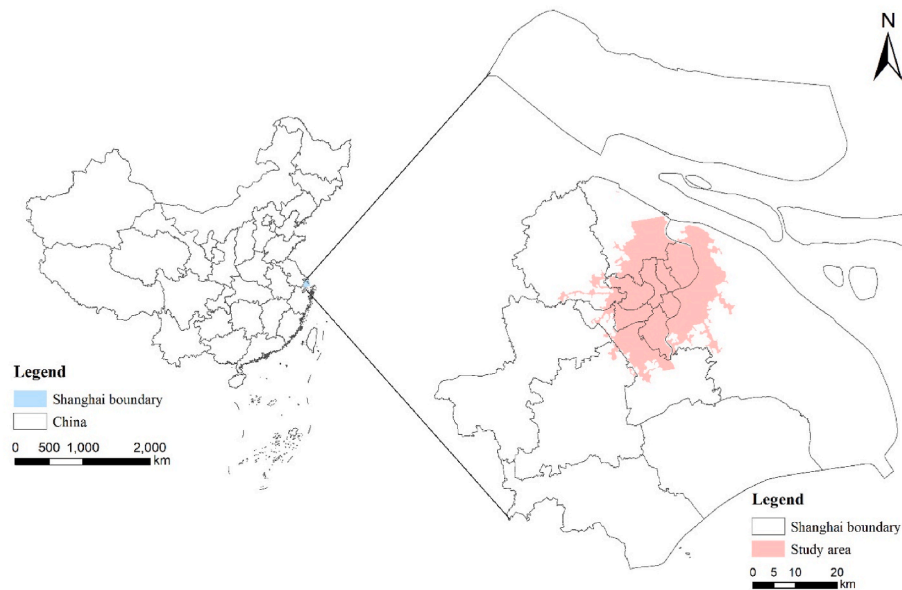
Fig. 1. Overview of the study area.

the core urban areas that had been construction land since the year of 2000. The fragmented and scattered regions that might belong to traditional county town centers were eliminated in comparison to existing core urban areas. The city in this study referred to the core urban region, which mainly involved 13 municipal districts with an area of 640 m^2 (Fig. 1). The proportion of major functional areas was sorted as follows: Residential (49.15%) > Industrial (16.34%) > Business office (7.61%) > Sport and cultural (5.63%).

2.2. Research data

2.2.1. RTCE spatial distribution mapping

The initial CO_2 emissions in this study came from the Global Carbon Grid v1.0 of the Global Infrastructure Emissions Database (GID) produced by Tsinghua University's Department of Earth System Science (http://gidmodel.org.cn/) [24]. The Global Carbon Grid v1.0 provided a global $0.1° \times 0.1°$ CO_2 emissions map in 2019 from energy use across six sectors, including emissions from the power, industrial, residential, road transportation, shipping, and aviation sectors. Residential and land transportation emissions data were from the International Energy Agency (IEA). They were interpolated into the corresponding raster pixels based on population density and road network data of different levels (e.g. county road, highway, etc.). The weights of the emissions from passenger road vehicles and freight trucks on the county road are 80% and around 15% [25]. Moreover, due to the air pollution control policy, Shanghai implements the driving restriction policy in the urban core region. The traffic emissions in the central area mainly comes from the emission generated by residents' travel.

Since residents' choices and behaviors could be impacted by urban form characteristics, the emissions of housing and travel transportation sectors directly related to residents' behaviors were selected as the research object. The residential and land transportation emissions of GID were added. Next, we created the finer resolution RTCE map than the GID to be appropriate for the city-level analysis. The Luojia 1-01 night light image data as a proxy variable, of which the spatial resolution is about 130 m, was used to generate a 130 m resolution RTCE map

[26]. The night time light data of China were derived from 275 images of Luojia 1-01 taken from June to December 2018, with a median error of less than 0.983 pixels in positioning accuracy (http://59.175.109.173:8888/app/login_en.html). We used digital number (DN) values which is the radiance value of the night time light remote sensing image as weights to allocate CO_2 emissions in the Luojia grid. DN is related to the radiation resolution of the sensor, the emissivity of the ground object, the atmospheric transmittance, and the scattering rate.

2.2.2. Data used for LCEZ construction

According to literature research, we chose six indicators of external morphology (i.e., building height (BH); building shape Index (LSI)), internal characteristics (i.e. functional mixed entropy (FME); road intersection density (RI)), and development intensity (i.e., road density (RD); building density (BD)) to describe urban form in the study area. They were calculated based on building contour data, road network data, and Points of Interest (POI) data with spatial attribute information in 2018 [13]. In addition, the urban boundary data is derived from the GUB dataset. Land use data was used the 30 m spatial resolution global land cover classification system V1.0 (GLC FCS30-2020) created by the Institute of Aerospace Information Innovation, Chinese Academy of Sciences [27]. The data of functional area types are derived from the EULUC-China data set [28]. The population density data is derived from the Unit Nation 2020 population density data set. The detailed description of all the data and their sources are reported in the Appendix Table S1.

2.3. Methodology

2.3.1. RTCE grid map downscaling interpolation

The GCS WGS 1984 geographic coordinate system of GID and Luojia 1-01 data were uniformed into the UTM Zone 48–52 coordinated system and WGS 1984 datum. Road intersections were chosen as the control points to match GID with Luojia data using the Arcmap10.5 geographic reference tool. Three to twelve control points with residual errors of less than one grid resolution were uniformly marked in the whole study area.
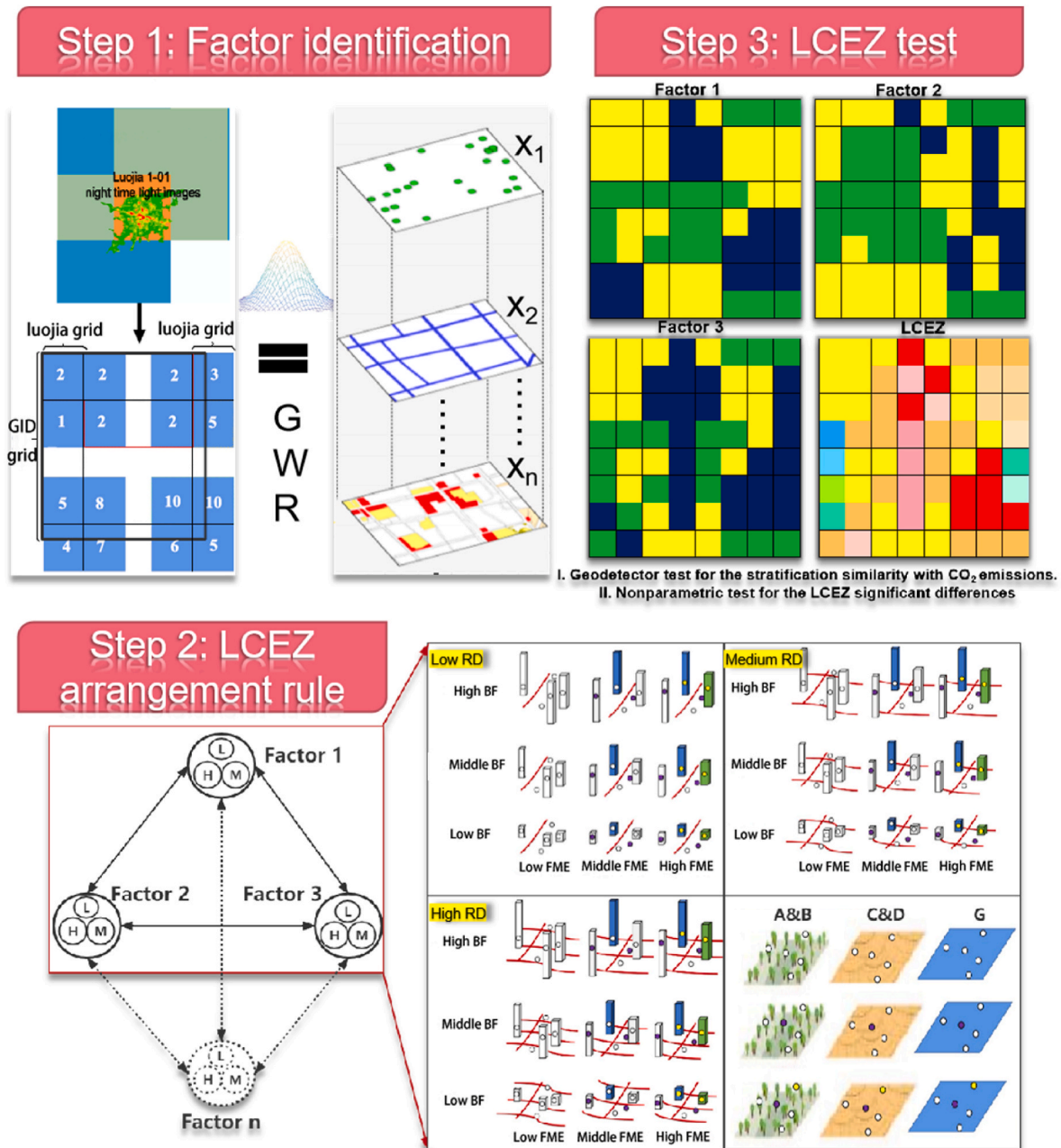
Fig. 2. The flowchart of the LCEZ construction. Step 1: Luojia1-01 night light image data is the proxy variable of the RTCE map. GWR is geographically weighted regression. Step 2: L is low. M is medium. H is high. the solid line is the three key factors. The dotted line means that n key factors can be selected in the future. The point is POI. the column is BF. the line is RD. A&B represents Dense&sparse forests. C&D represents Farmland&grassland&wetland. G represents the water body.
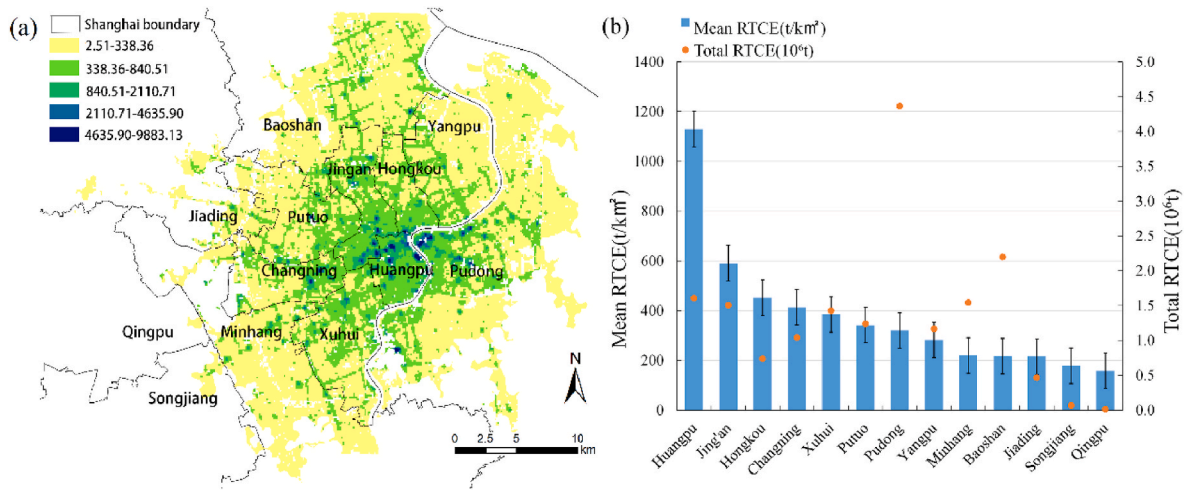
Fig. 3. (a) Spatial distribution of RTCE. (b) The mean (left axis with bar and standard error) and total (right axis with point) RTCE in Shanghai 13 districts.

The CO_2 emission of each Luojia grid was calculated as follows.

$$C_i = \frac{DN_i}{DN_j} \times C_j \tag{1}$$

$$DN_j = \sum_1^k DN_{i,1} + \ldots + DN_{i,k} \tag{2}$$

Where C_i is the CO_2 emission of Luojia 1-01 grid i. DN_i is the nighttime light brightness of the Luojia grid i. DN_j is the nighttime light brightness of GID grid j and is the sum of all Luojia 1-01 grids in the 0.1°grid. C_j is the total CO_2 emission of GID grid j. Since the uncertainty source of LCEZ

Fig. 4. Spatial distribution of hot and cold spots of residential and transport CO_2 missions.

construction would be brought by the downscaling interpolation using the night time light images. We reported the R^2 between the CO_2 and DN values of the Luojia data in the study area as a metric for the LCEZ validation, which is 0.692 of the equation $y = 0.0057x + 7.1096$. Global Moran's I index measures the autocorrelation of the RTCE spatial pattern. The values were between −1 and 1. Values between 0 and 1 show the spatial positive correlation pattern. Values between −1 and 0 show the negative correlation pattern.

2.3.2. Parameters system of LCEZ

The BH and the LSI of the external form were selected. Floor information from building contour data represented the building height. The shape index was calculated by the vector polygon of building contour data. Larger shape index values indicate more complex patches.

The FME and the RI of internal characteristics were selected. The mixed degree of urban functional area was calculated through the point of interests (POI). In this study, information entropy was used to calculate the mixed degree of urban functional areas according to POIs. The information entropy can be used as a measure of the complexity of a system [29]. If the system is more complex and the types of different situations are various. The information entropy is relatively large. If a system is simple. There are a few types of situations, and the information entropy is small. The higher the information entropy value is, the higher the mixing degree is.

The network data were used to calculate the RI through the network analysis tool and spatial connection tool in ArcMap 10.5.

The RD and the BD index were selected for urban development intensity, which could be calculated through road network data and building contour data (Table 1).

2.3.3. LCEZ construction

The objective of LCEZ construction was to classify regions with similar form characteristics into homogeneous regions based on the vital urban form factors that affect RTCE. The LCEZ could help summarize the composition and configuration of low-carbon urban form patterns and discover the general rule of urban form factors that affect CO_2 emissions to provide the scientific basis for low-carbon urban planning practice.

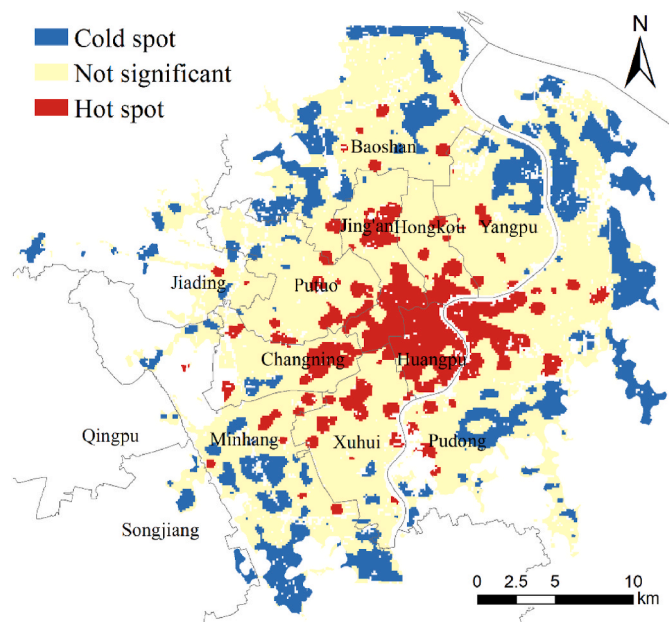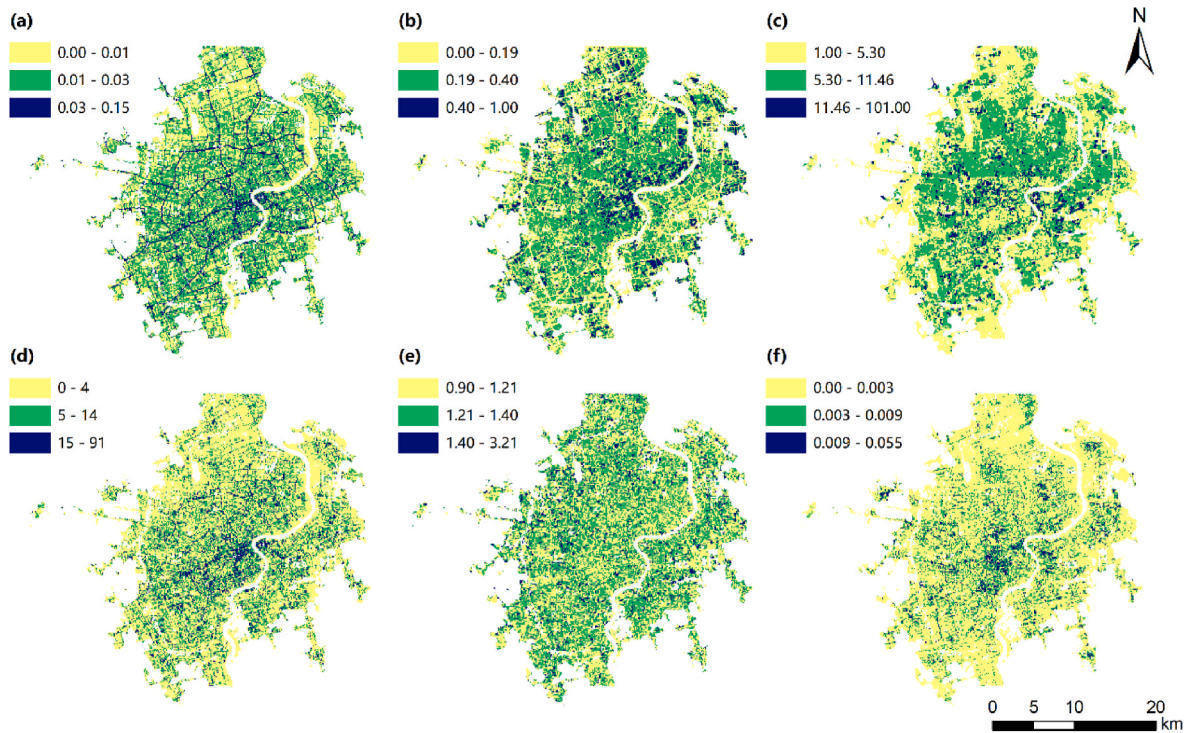#### 2.3.3.1. Parameters screening. Firstly, because of the spatial

Fig. 5. Spatial distribution map of the Urban morphology factor. (a) is the RD, (b) is the BD, (c) is the BH, (d) is the RI, (e) is the LSI, and (f) is the FME.

Table 1
The calculation formula of 6 key factors.

Three perspectives	factors	Calculation equation	Formula explanation
External form	BH	NA	There is the floor number information.
	LSI	$LSI_i = \frac{S_i}{2\sqrt{\pi A_i}}$	LSI_i is the building outline shape index on the grid i; S_i is the perimeter of the building; A_i is the area of building patches on the grid i.
Internal characteristics	FME	$FME = \frac{H_s}{A_i}$	H_S is the spatial information entropy of the MN^{th} grid (For the details, please find Appendix A); A_i is the area of the grid.
	RI	Network analysis tool and spatial connection tool in Arcmap10.5	
Urban development intensity	RD	$R_d = \frac{L_{mn}}{s}$	R_d is road density; L_{mn} is road length in grid (m); S is grid area (m²)
	BD	$B_d = \frac{BA_{mn}}{s}$	B_d is building density; BA_{mn} is building area in grid (m²); S is grid area (m²)

heterogeneity and autocorrelation of urban form characteristics [29–31], we used the GWR model considering the local regression relationship to explore the influence of six urban form factors (BH, LSI, FME, RI, BD, and RD). The GWR model provided the coefficient of determination (R^2) and regression coefficients between RTCE and urban form factors. The positive and negative regression coefficients illustrated the direction of the effects of the urban form index on RTCE. The key representative factors affecting RTCE were selected by the absolute value of average regression coefficients. The variance inflation factor (VIF) index was used to determine the multicollinearity to avoid the analysis deviation caused by the interaction among urban form factors.

The GWR was widely used in the research of spatial econometrics, criminal exploration, and environmental pollution mapping [32–35]. It expands the connotation of the linear regression model, reflects the change of spatial position of regression coefficients β and i, and explores the mechanism of the influence of explanatory variables on explained variables with the change of spatial position.

$$y_i = a_0(u_i, v_i) + \sum_k a_k(u_i, v_i)X_{ik} + \varepsilon_i \qquad (7)$$

Where y_i is the variable being explained variable on grid i, X_{ik} is the kth explanatory variable on grid i, ε_i is the residential, (u_i, v_i) is the location of grid i, $a_k(u_i, v_i)$ is the kth regression coefficient of grid i.

2.3.3.2. LCEZ construction. Firstly, the important factors affecting RTCE (e.g. BH, FME, RD) were selected according to the average regression coefficient of each factor in the GWR model. Secondly, the selected factors were divided into high, medium, and low categories and were combined to construct the LCEZ. The number of the selected factors was n. The LCEZ categories was 3^n. If three factors were filtered, 27 LCEZ categories would be constructed. The FME factor that can be reflected in the natural vegetation cover land (e.g. farmland, shrub and grass, and water body) could be used to construct the LCEZ of natural vegetation cover land. The factors depicting the building and road network were only used on the construction land.

According to GLC_FCS30-2020, the natural vegetation cover land of the study area was divided into dense & sparse forest (LCEZA&B), farmland & grassland & wetland (LCEZ C&D), and water body (LCEZG). LCEZA&B is the closed evergreen broad-leaved forest. LCEZ C&D is dry land, herb land, irrigated farmland, grassland, or wetland. The three types of natural vegetation cover lands were combined with the high, medium, and low levels of FME respectively to construct 9 LCEZ types of natural vegetation.

2.3.3.3. Verification and analysis of LCEZ. Finally, we used two methods to verify the LCEZ results. Firstly, the multi-independent sample nonparametric test method was used to test the different significance of

Table 2
The collinearity test for the LCEZ parameters.

Urban form factors	VIF	T = 1/VIF
BH	1.060	0.943
LSI	1.012	0.988
FME	1.152	0.868
RI	2.126	0.470
RD	2.147	0.466
BD	1.081	0.925

Table 3
GWR results of the LCEZ parameters.

Urban form factors	Average regression coefficient ± Standard errors	R^2	R^2 Adjusted
BH	0.027 ± 0.13	0.50	0.45
LSI	−0.0025 ± 0.063		
FME	0.032 ± 0.072		
RI	−0.0046 ± 0.058		
RD	0.025 ± 0.054		
BD	0.00021 ± 0.027		

different types of LCEZs. Nonparametric test infers the shape of the population distribution by sample data when the population variance is not uniform and the samples are not in the normal distribution. The Kruskal-Wallis H test method in SPSS software was used to test whether there were significant differences between LCEZs. If the progressive significance is less than the level of 0.05, it indicates that there are significant differences among different regions.

Secondly, the similarity verification of the LCEZs was carried out using GeoDetector. GeoDetector is originally used to analyze the relationship between local disease risk and relevant geographical factors. It's a statistical method to detect spatial heterogeneity and reveal the causal relationship. The major advantage of GeoDetector is that independent variables can be numerical and categorical.

The RTCE was the dependent variable, while LCEZs were the independent variables. The factor detector module analyzed the extent to which factor (x) explains the spatial heterogeneity of RTCE (y) in the study area. The q value of the factor detector ranges from 0 to 1. The larger the q value is, the stronger the factor explains the spatial heterogeneity of RTCE.

$$q = 1 - \frac{\sum_{h=1}^{L} N_h \sigma_h^2}{N\sigma^2} \tag{8}$$

Where h is the type of LCEZ in the study area, N is the number of all zoning types, N_h is the number of LCEZ types in the layer h, σ^2 is the variance of RTCE in the study area, σ_h^2 is the variance of layer h. The logarithm was used to smooth the wide distribution range and extreme values in RTCE values.

To explore the main urban form characteristics of low RTCE clustered areas under different urbanization levels, the local Getis G_i^* with a 95% confidence interval was used to identify the cold (Low-Low cluster) and hot (High-High cluster) spots areas of the RTCE. The cold spot area is the low-low cluster area, which represents the low RTCE clustered areas. The hot spot area is a high-high cluster area, which represents the high RTCE clustered areas. The LCEZ characteristics in different urban functional areas of the cold spots areas were analyzed in terms of the different population densities. According to the distribution area and spatial pattern of different LCEZs, the key form index and their value ranges that should be considered in the detailed urban planning at the block scale were expounded (Fig. 2).

3. Results and analysis

3.1. RTCE spatial pattern

Based on the RTCE map, there are significant differences in the intensity and sum of RTCE in 13 districts of Shanghai. Pudong and Baoshan were the first and second greatest regions in the total emissions, which were $4.4 \times 106t$ and $2.2 \times 106t$, respectively (Fig. 3). Songjiang and Qingpu had the smallest total missions ($0.07 \times 106t$ and $0.01 \times 106t$) and mean emission intensities (178.5 t/km2 and 158.4 t/km2).

From the perspective of average emission intensity, the intensities of Huangpu (1129.5 t/km^2), Jing'an (590.7 t/km^2), Hongkou (451.9 t/km^2), and Changning (413.7 t/km^2) were high with the large standard errors. The intensities of Xuhui, Putuo, Pudong, Yangpu, Minhang, Baoshan, and Jiading were between 200 t/km^2 and 400 t/km^2. Excepting for Songjiang and Qingpu, the intensities of other regions all exceeded 200 t/km^2. It's worth noting that Pudong's average emission was at the medium level, but the total emission was the largest.

The Moran's I of the RTCE was 0.62, showing a positive spatial correlation and a spatial aggregation pattern. The spatial correlation was strong. Both global and local spatial autocorrelation showed significant statistical spatial characteristics. The hot spot analysis results showed (Fig. 4) that there were 13.30% hot spots and 20.88% cold spots in the study area under the 95% confidence interval. Hot spots regions were mainly in the center of the study area (e.g. Huangpu, Xuhui, Changning, Putuo, Jing'an, and the western area of Pudong district). Cold spots were mainly distributed in the surrounding areas, such as the northern area of Yangpu, the northern and southeastern area of Pudong, the southern area of Minhang, and the northern and western areas of Baoshan.

3.2. LCEZ construction result

3.2.1. Morphological characteristics of the study area

The BH (floor/km^2) parameter was divided into low (1–5.30), medium (5.30–11.46), and high (11.46–101.00). The high values are mainly distributed in the Pudong and Putuo districts. The median values are mainly distributed in Jing'an, Hongkou, Yangpu, and Minhang. The low values are mainly distributed in Huangpu and Jiading. The LSI was divided into low (0.90–1.21), medium (1.21–1.40), and high (1.40–3.21).

The FME reflects the mixed degree of urban functions in a certain region. The three categories of FME were low (0-3.00 × 10^{-3}), medium (3.01 × 10^{-3}-9.00 × 10^{-3}), and high (9.01 × 10^{-3}-5.50 × 10^{-2}). The high values are mainly distributed in Huangpu, Xuhui, Jing'an, and Pudong. While the medium and low values were mainly in Baoshan, Hongkou, Putuo, Jiading, Minhang, and Changning. The RI (per/km^2) was divided into low (0–4), medium (5–14), and high (15–91).

The RD (m/km^2) was divided into low (0–0.01), medium (0.01–0.03) and high (0.03–0.15). Huangpu and Pudong were the main areas with high RD, while other areas had median and low road density. The BD (m^2/km^2) was divided into low (0–0.18), medium (0.18–0.41), and high (0.41–1.00) (Fig. 5).

3.2.2. Screening results of LCEZ parameters

The VIF values of each urban form index were all less than 10, indicating that there was no collinearity relationship among the six factors [36] (Table 2).

The average regression coefficients of each factor had great differences with the big standard deviation changes (Table 3). The result indicated that the influence power and trend of each factor are various in different regions. The coefficient of determination (R^2) of GWR was 0.45, indicating that the comprehensive explanatory power of the six selected factors on RTCE was close to half. The positive and negative GWR regression coefficients illustrated the effect direction of the urban form factors on the RTCE. The regression coefficients of BH, FME, RD,
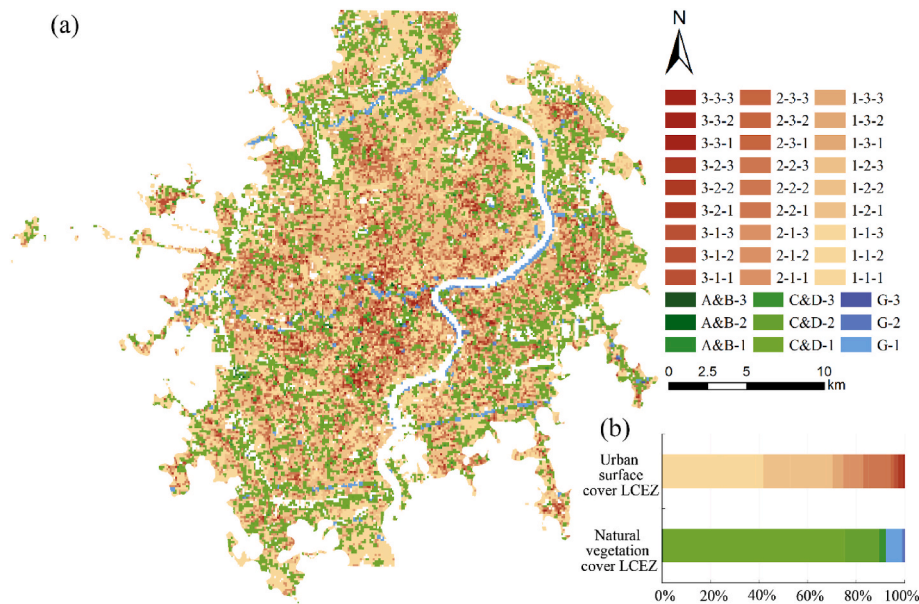
Fig. 6. (a) Spatial distribution map of the LCEZ (b) proportion of LCEZ area.

Table 4
The factor detector of GeoDetector result of the LCEZs in the urban surface and natural vegetation lands.

LCEZ type	Urban surface land	Low FME	Medium FME	High FME
Factor detector (q value)	0.121**	0.073**	0.061**	0.122**
LCEZ type Factor detector (q value)		Low BH 0.085**	Medium BH 0.066**	High BH 0.154**
LCEZ type Factor detector (q value)		Low RD 0.061**	Medium RD 0.058**	High RD 0.077**
LCEZ type	Natural vegetation land	Dense & sparse fores	Farmland & grassland & wetland	Water body
Factor detector (q value)	0.051**	0.112**	0.045**	0.061**

Note: ** represents P-value <0.01.

and BD were positive, which indicates that the increase of these factors would lead to the increase of RTCE. The absolute values of the regression coefficients of FME (0.032), BH (0.027), and RD (0.025) had far greater influences than the others' (Table 3). Therefore, we selected these three factors combined with the land use/land cover data of Shanghai to construct the LCEZ.

3.2.3. LCEZ spatial pattern

For the urban surface land, the low FME type of the LCEZ accounted for the largest proportion (75.64%) (Fig. 6). For example, LCEZ 1-1-1 accounted for 25.56%. The medium FME type of the LCEZ was the second (20.03%). For example, LCEZ 2-2-2 accounted for 6.95%. The high FME type of the LCEZ was the smallest (4.33%). For example, LCEZ3-2-2 accounted for 1.49%. For the natural vegetation cover land, farmland, grassland, and wetland occupied the largest area (91.84%). The proportions of LCEZC&D-1 and LCEZC&D-2 were 75.40% and 13.84%, respectively. Water LCEZ G was the second (7.77%), in which

LCEZ G-1 accounted for 6.79%. The area of LCEZ A&B in dense and sparse forest was the smallest (0.39%), in which LCEZ A&B-1 accounted for 0.21%.

3.2.4. LCEZ verification result

The Kruskal-Wallis test results of the LCEZs in urban surface land demonstrated that the asymptotic significance was 1.0×10^{-6} and the Chi-square value was 4187.38. In the natural cover land, the asymptotic significance was 1.0×10^{-6} and the Chi-square value was 507.72. The results indicated that the different types of LCEZ were significant difference. The factor detector of GeoDetector showed that the similarity of LCEZs in urban surface land (q = 0.121) was higher than that in natural vegetation land (q = 0.051). The similarity of LCEZs in high values regions of three selected factors (BH, FME, and RD) was higher than that in low value regions, and much higher than that in medium regions (Table 4).

3.3. LCEZ characteristics and distribution in cold spots of the RTCE map

The cold spots areas represented the low RTCE areas. We summarized urban form characteristics of the cold spots areas to help the low-carbon urban planning practice (Fig. 7). According to the different population densities, the cold spots areas were divided into low, medium, and high population density areas.

In low population density areas, 1-1-1, 1-1-2, and 1-1-3 accounted for 53.56%, 16.46%, and 0.69%. In each functional area, 1-1-1 always accounted for more than one-third of the total area. The residential zone was the largest functional type (52.53%) in the study area, with 34.79% of 1-1-1, 16.68% of 1-1-2, 12.87% of 1-2-1, and 15.65% of 1-2-2 type. Similarly, 1-1-1 (63.76%) and 1-1-2 (13.81%) types were the major type for the industrial zone, followed by 1-2-1 (12.10%) and 1-2-2 (5.23%) types. As to Business office zone, 1-1-1 (41.44%) and 1-1-2 (19.37%) types accounted for the largest proportion of the total area, followed by 1-2-2 (15.06%%), 1-3-2 (7.53%), and 2-1-1 (7.53%) types. In the sport and culture zone, 1-1-1 (53.23%) and 1-1-2 (12.79%) types were also the major types, followed by 2-1-2 (9.45%) and 1-2-2 (6.16%) types. In addition, the average proportion of the medium FME LCEZs in some functional zones was relatively large, such as in commercial service zone (8.33%), administrative (11.32%), educational (15.67%), and park & greenspace (13.65%). Generally, 1-1-1 (53.56%) and 1-1-2 (16.46%) types accounted for the largest proportion of all functional areas,
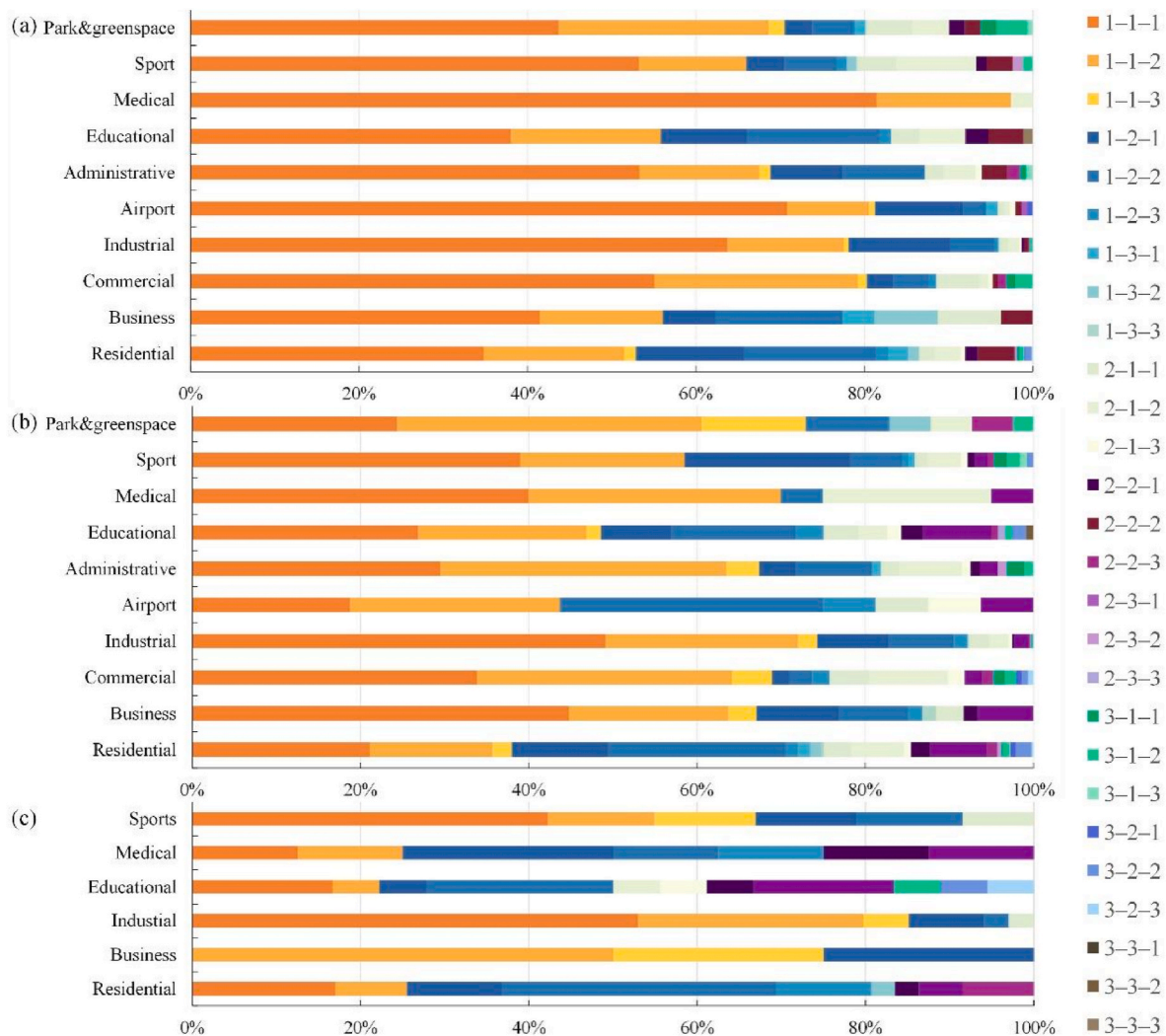
Fig. 7. Area proportions of different types of LCEZs in different populations of cold spot (a) is the low population, (b) is the medium population, (c) is the high population.

followed by 1-2-1 (7.13%) and 1-2-2 (7.95%) types.

In medium population density areas, the average percentages of LCEZs with low, medium, and high FME were 81.84%, 15.89%, and 2.26%, respectively. In the residential zone, 1-1-1 and 1-2-2 types accounted for 21.12% and 21.10%, respectively, followed by 1-1-2 (14.62%) and 1-2-1 (11.48%) types. The proportions of industrial, business office, and sport & cultural zones were similar to that of residential zones, with 1-1-1 (49.19%, 44.78%, 38.98%), 1-1-2 (22.83%, 18.99%, 19.56%), 1-2-1 (8.47%, 9.77%, 19.69%), and 1-2-2 (7.78%, 8.27%, 6.12%) types. Generally, LCEZs with low FME were still the main types in medium population areas. The main types were 1-1-1 (32.75%), 1-1-2 (25.15%), 1-2-2 (11.58%), and 1-2-2 (6.41%) types.

In high population density areas, the average percentages of LCEZs with low, medium, and high FME were 82.84%, 14.38%, and 2.78%, respectively. In the residential zones, 1-2-2 and 1-1-1 types accounted for 32.51% and 17.00%, respectively. While 1-2-1 and 1-2-3 types both counted for 11.33%. In industrial zones, 1-1-1 (52.97%) and 1-1-2 (26.74%) types accounted for the largest proportion, followed by 1-2-1 (8.91%) and 1-1-3 (5.43%) types. There were only the low FME LCEZs (50% of 1-1-2, 25% of 1-1-3, and 25% of 1-2-1) for the business office zone. In sport & culture zones, the major LCEZ types were 1-1-1 (42.28%), 1-1-2 (12.68%), and 1-2-2 (12.68%). In line with the low and medium population density areas, 1-1-1 (23.57%), 1-1-2(19.33%), 1-2-1(14.62%), and 1-2-2(13.81%) types were the principle types in

high population areas.

3.4. LCEZs with low FME–main LCEZ types in the study area

In the cold spots area, the LCEZs with low FME (1-1-1, 1-1-2, 1-1-3, 1-2-1, 1-2-2, 1-2-3, 1-3-1, 1-3-2, 1-3-3) were the principle types which accounted for 84.31%. The main urban form characteristic of these LCEZ types was that the change trend of BD and RD was opposite (Fig. 8). When LSI, FME and BH remained unchanged, BD gradually decreased with the gradual increase of RD and RI. While FME and RD, LSI, and RI remained unchanged, BD changed slightly as BH increased.

When the mixed degree was low (FME≤0.0029), the urban pattern of the compact low-rise low network (1-1-1), mid-compact low-rise mid-network (1-1-2), compact-mid rise-low network (1-2-1), and mid compact-mid rise-mid network (1-2-2) occupied a large proportion in the cold spots areas of RTCE. The 1-1-1 and 1-1-2 types had the same range of floor heights [1, 5.30], and 1-2-1 and 1-2-2 had the same range of floor heights (5.30, 11.44). The road density of 1-1-1 and 1-2-1 was less than 0.014 (m/km^2), and that of 1-1-2 and 1-2-2 ranged from 0.014 to 0.032 (m/km^2) (Table 5).
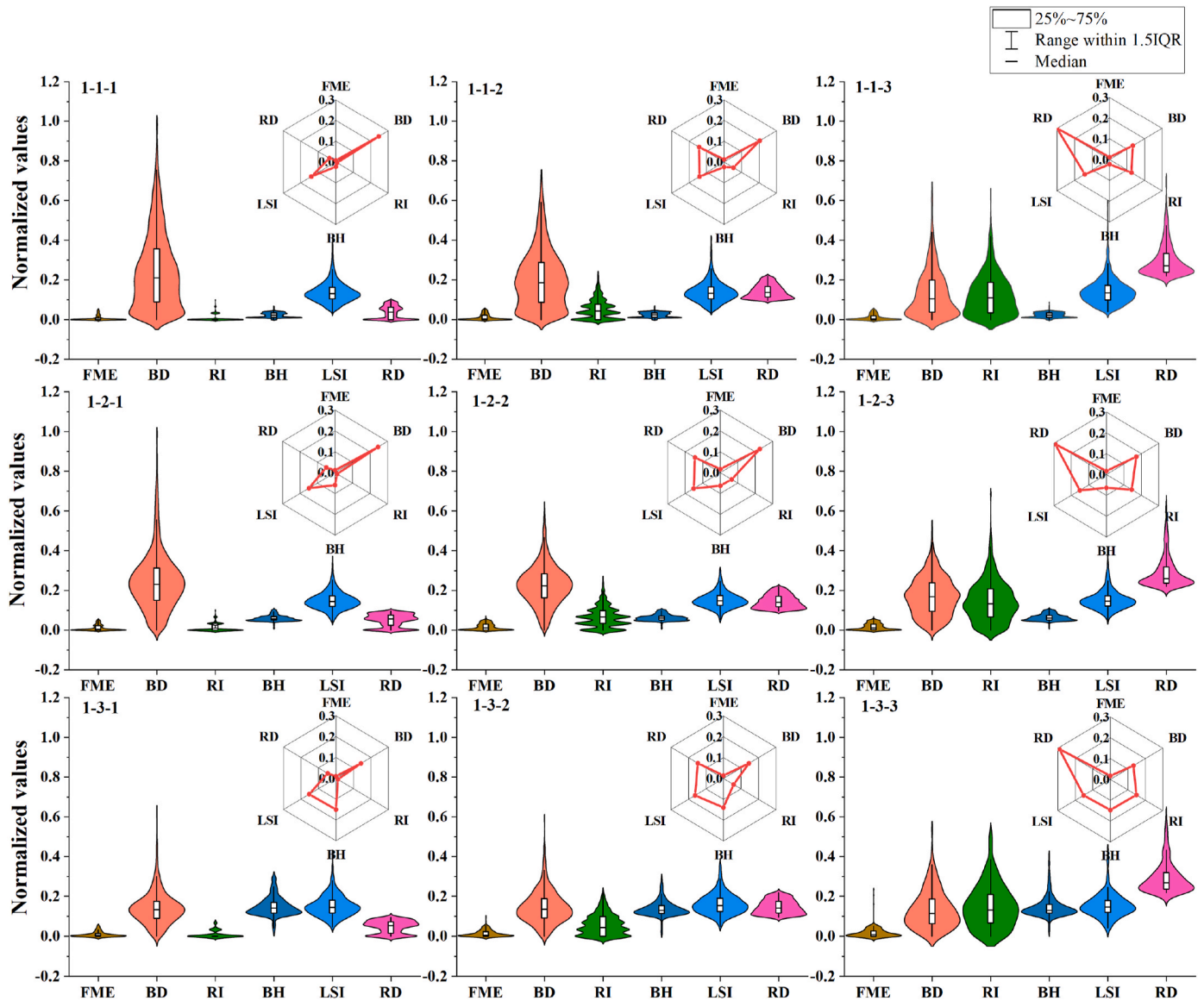
Fig. 8. The urban form characteristics of the LECZs with low FME.
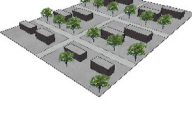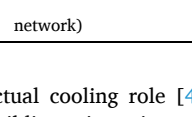
4. Discussion

4.1. The key urban form indicators for the RTCE

In this study, BH, FME, and RD selected based on the GWR model were the key urban forms affecting RTCE in the core urban area of Shanghai. BH had a positive impact on CO_2 emission [37], which was consistent with our results that the average regression coefficient of BH in the GWR model was positive. From the perspective of individual building heat dissipation and heating, the large building surface area results in energy use (3-dimensional). The higher the building, the more solar energy it receives, further increasing the risk of overheating. Besides, the operation of ventilators and elevators, which increase the use of energy, offsets the energy savings from the increased hours of light [38]. Moreover, BH was also the main factor in constructing the LCZ partitioning method. From the perspective of internal factors, the mixed degree of land use type and functional area, which directly affects residents' travel choice and efficiency, has a great impact on CO_2 emission. This study found that the effect of FME on RTCE was positive in most of the study areas, which indicated that the increase of FME would lead to the increase of RTCE. Despite this, the study used GWR to analyze the

relationship between urban form and RTCE in 31 major urban centers in China and found that the influence of increasing FME of urban functional areas on urban RTCE showed an exponential downward trend [13]. From the perspective of development intensity, RD reflects the CO_2 emission reduction from the efficiency improvement brought by the urban scale effect. However, excessive aggregation will bring diminishing marginal benefits of efficiency, resulting in high emissions. Therefore, the effect direction of RD on RTCE is mainly positive, which is consistent with the results of this study.

Two of the selected factors representing external characteristics and development intensity formed different building configurations, such as compact-low rise-low network and compact-medium rise-low network. Studies of building configuration showed that dense buildings may reduce the incoming airflow and the efficiency of urban ventilation. Dense buildings absorbed more solar radiation and store more heat than the sparse buildings, which increased surface temperatures. On the other side, buildings also provided shade to effectively improve the thermal environment of the street valley. However, the shading intensity of buildings was greater than that provided by street trees [39]. Because when the buildings and trees overlapped, the shading of trees will be covered by buildings, resulting in the trees being unable to play the

Table 5
The urban form feature values for the selected LCEZ.

LCEZ type	Characteristics' reference values	
	Urban form factor	LCEZ range
LCEZ1-1-1 (compact-low rise-low network)	FME (NA)	(0, 0.0029]
	BH (floor/km^2)	[1, 5.30]
	RD (m/km^2)	(0, 0.014]
	BD (m^2/km^2)	(0, 1.00]
LCEZ1-1-2 (mid compact-low rise-mid network)	FME (NA)	(0, 0.0029]
	BH (floor/km^2)	[1, 5.30]
	RD (m/km^2)	(0.014, 0.032]
	BD (m^2/km^2)	(0, 0.95]
LCEZ1-2-1 (compact-mid rise-low network)	FME (NA)	(0, 0.0029]
	BH (floor/km^2)	(5.30, 11.46]
	RD (m/km^2)	(0, 0.014]
	BD (m^2/km^2)	(0, 1.00]
LCEZ1-2-2 (mid compact-mid rise-mid network)	FME (NA)	(0, 0.0029]
	BH (floor/km^2)	(5.30, 11.46]
	RD (m/km^2)	(0.014, 0.032]
	BD (m^2/km^2)	(0, 0.83]

actual cooling role [40]. Therefore, it's better to set the reasonable building orientation and building-street aspect ratio and optimize street tree size and spatial distribution pattern to effectively improve the comprehensive shading and cooling effect. In urban street canyons, dense buildings caused temperatures to rise from 3 °C to 7 °C [41]. It was found that increasing the building-street aspect ratio ($0.2 < H/W < 2.2$) could transcend the climatic background and had an absolute impact on the geothermal environment [42]. In addition, the attributes of dense buildings changed the way residents met their basic living needs and energy use habits and further altered the residents' CO_2 emissions [43]. RD of this study was calculated based on the road length. The low RD represented the large area of the building cluster. We found that the average RD and BD of all LCEZ types in the cold spot areas were inversely correlated, which showed the average low RD high BD or high RD low BD. The LCEZ types with low RD and high BD were major, indicating that the clustered architectural groups were in a contiguous form and the size of the building aggregation was large in the study area.

In addition, FME representing the internal characteristics was the most important factor affecting RTCE. At the individual and household scale, many studies believed that mixed entropy of functional zone and mixed degree of land use affected travel cost (distance and time) and residents' travel decisions, and thus had a great impact on urban residents' CO_2 emissions from transportation. Even after controlling for travelers' preferences and residents' self-selection, the urban form influence on travel was significant [44], and was more than 50% on vehicle mileage and some other travel behaviors [45]. Moreover, vehicle travel and related emissions were influenced not only by local urban form factors but also by the far geographical environment [46]. Therefore, CO_2 emissions from multi-function zones may be higher than those from single-function zones.

4.2. The division methodology and the significance

LCEZ classification is similar to the design of a stratified sampling box which is typically based on the feature or identification of the analysis unit. Since Tobler's First Law of Geography could be applied to geographical research objects. Everything is related to everything else, but near things are more related to each other. The division methodology is mainly determined by the existence of prior knowledge and experience (PKE) and historical reference data (HRD) [47]. If neither information is available, the simple method would be used. If there is only PKE, it will be the correlation factor division method. If only HRD is available, it would be better to use the data-driven division method. If both PKE and HRD are present, the division method will be combined with supervised and unsupervised learning division methods. The objective of supervised learning is to explore the correlations among variables to select the features, including feature selection method (e.g. Principal Component Analysis, Linear Correlation Analysis, Information Entropy, Attribute Importance) and prediction model (e.g. General Linear Regression, Spatial Regression, Machine Learning Algorithm). Non-supervised learning to calculate the similarity of spatial pixels and then clusters to obtain division results. Common methods include K-Means, BRICH, DBSCAN, and STING. There were both PKE and HRD in this study. Therefore, the Spatial Regression model was used for supervised learning. Three key feature factors were selected according to GWR mean regression coefficients. Then Jenks classification method and combination method for a few key factors ($n < 3$) were used to construct the LCEZ. If there were more than three key factors, an unsupervised learning method would be recommended. This study also implemented the K-Means unsupervised method for the LCEZ construction in the pre-experimental stage. According to GWR analysis results, the main local driving factors of each grid were selected. Next, K-Means was used to get the divisions based on 20 different driven types (such as FME-RD-BH, FME-RD-LSI). However, the factor detector of the GeoDetector found that the performance of K-Means LCEZs was similar to the Jenks method (Appendix Table S2). Therefore, the results obtained by the complex supervised and unsupervised division methods were not necessarily better than those obtained by simple supervised and intuitive LCEZ division method. In general, in addition to considering the building shape and underlying surface characteristics, LCEZ also incorporated the internal characteristics of FME information. The main goal was to better understand the impact of urban form on RTCE. LCEZ with adequate accuracy would help provide implications for the practical operability of low-carbon city planning, identify the key urban form factors (e.g. FME) to favor the building level energy simulation, complement the geometric factors (e.g. building height and density) into urban energy model simulations [48].

4.3. LCEZ implications

In the study area, when FME was low, the compact and mid-compact urban forms, the medium and low road network, and building height occupied a large proportion in the low RTCE accumulation area. The study carried out in the Yangtze River Delta urban agglomeration found that compact mid and high rise buildings should be clustered together to reduce CO_2 emissions, but the size should be limited. Compact mid-rise building was the common and important urban form, usually with

commercial and residential functions [20]. This result was similar to our result that high BD was the main direction of the future development of highly urbanized areas. The compact mid rise buildings are related to low carbon emissions.

The LCEZs were constructed based on the existence of the stock urban form. The recommended urban form featured values could be used for both the urban new construction plans and the renovation projects. However, the renovation and revitalization of existing communities often involve multi-dimensional considerations and complex processes, including the difficulty of relocation, physical appearance, cultural heritage, and urban function. Therefore, the recommended urban form featured values are better suited for new constructions. The process of planning and constructing new communities involves the 4 steps in China. Firstly, during the land use planning approval phase, the natural resources and plan department approves the construction plan according to the land use master plan, land supply policy, and land use standards. Next, the governments of district and county level and land construction parties jointly formulate the detailed planning plan of the new construction project with the urban planning department. The architectural design unit designs the residential, commercial, public facilities, and other buildings in the new urban area. Thirdly, the natural resources and plan department approves the detailed plan. Meanwhile, the Environmental Protection Department examines the environmental impact assessment to ensure compliance with environmental requirements. Therefore, the natural resources and planning department could set urban form featured values for the construction of low carbon constructions through the local standard, construction guidance, and regulation. Finally, the urban administration department oversees construction and conducts final acceptance inspections to ensure project compliance with relevant standards. At present, the natural resources and plan department has considered factors including building shape, building height, and lighting layout in the approval process. In the future, to achieve the "Double Carbon" target, it may consider increasing the indicators favoring the carbon emission abatement.

We recommend the different LCEZ types in the various functional zones. The 1-1-1, 1-1-2, 1-2-1, and 1-2-2 were the main LCEZ types in the residential zone, which is the largest functional zone in core urban area. The characteristics of these four types were low mixed degree (FME<0.0029), mid compact, medium, and low rise (BH = 11–12 floor) type. For the business office functional area, 1-1-1, 1-1-2, 1-2-1, and 1-2-2 were also the major types. In addition, the medium FME types (e.g. 2-1-1, 2-1-2) also occupied a large proportion. In the Central Business District planning, it was suggested to use the low and medium mixed degree (FME<0.009), mid compact, medium, and low rise (BH = 11–12 floor) type. Industrial and sport&cultural zones were similar to residential zones. The results of this study provided insights into the design of basic urban forms, avoiding the urban form with high mixed (FME≥0.009), high building floor (BH ≥ 11.46), and high road density (BD ≥ 0.032).

As to the validation method, since the CO_2 emissions data were based on the energy use statistics and the proxy variables. Uncertainty exists. Before the actual application of the feature values of the LCEZs. It's better to use the stratified random sampling and the emission factor method to validate the results. There should be three steps. Firstly, the stratification was constructed based on selected major factors. The sample region was identified at the 90% confidence interval and 10% allowable errors. Secondly, the residential and transport CO_2 emissions were calculated through the activity level (AL) (e.g. energy use data) and emission factors. Finally, the low RTCE LCEZ types could be identified to validate the recommended low emission LCEZs (e.g. 1-1-1,1-1-2,1-2-1 and 1-2-2).

4.4. Strength and limitation

The advantage of this study was the consideration of the spatial heterogeneity for the key factors selection. Compared with ordinary

regression and machine learning algorithms, the results were appropriate for the characteristics of geographical objects after considering spatial heterogeneity and autocorrelation. After comparing the results of supervised and unsupervised division methods, a simple grouping method was proposed to construct LCEZ. The obtained LCEZ could help effectively analyze different urban morphological characteristics and provide scientific guidance for low-carbon planning practice. We carried out the study in the central urban area and identified the low carbon LCEZ types in the carbon emission cold spot regions which represent the low-low carbon cluster regions. These measures ensure the typicality and representativeness of the research results. Therefore, the recommended urban morphological characteristic values after verification can be directly applied in other highly urbanized areas. For suburban and exurban regions, it is necessary to repeat the whole procedure to reconstruct the LCEZ framework and calculate the corresponding urban form feature values.

This study also had the following three limitations. First, some morphological factors were sensitive to the change of scale. We planned to carry out a multi-scale analysis to obtain consistent application results at different scales in the future. Second, when selecting the influence factors of RTCE, the tele-influence brought by the urban pattern and mixed degree could be considered. The impact factors might be different in the study areas with different levels of urbanization. The results of this study only represented the main urban morphological characteristics affecting RTCE in highly urbanized areas. In the next step, we plan to conduct studies on different climatic regions and different levels of urbanization and summarize the rules for each type of location. Third, since RTCE affected by urban form is direct and indirect. It is more accurate to use the total energy use data emissions than carbon satellite or field monitoring data as analysis objects. Nevertheless, the night time light data is the most commonly used proxy variable for CO_2 emission downscaling mapping, there are also background noise [49], geographic positioning errors [50], and representational problems.

5. Conclusions

Based on the local spatial regression method (GWR), the key urban form factors of RTCE were selected. An easy LCEZ construction method framework was proposed. The results of LCEZ were applied to find the main urban form characteristics of different urban functional zones in the low RTCE area. The LCEZ types that could guide the practice of low-carbon city construction are recommended for the highly urbanized area.

The analysis showed that 1) half of the RTCE can be explained by six factors, which represent the urban external morphology, internal characteristics, and development intensity. FME, BH, and RD had a great influence on RTCE, and most of them were positive. 2) The LCEZ was constructed with a simple framework. The LCEZs of constructed surface and natural vegetation cover lands were significant difference. The representation of LCEZs of urban construction surface was higher than that of natural vegetation cover land. The q value rank of three key factors used to construct LCEZ was high > low > median value region. 3) In the RTCE cold spot area of the highly urbanized area, the LCEZ types with low FME of different population densities accounted for the highest proportion among all functional zones, followed by the LCEZ types with medium and high FME. The LCEZ types with low FME, mid and low BH, and mid and low RD were the main types in four major urban functional zones (residential, industrial, business office, and sport&cultural). Therefore, in the detailed planning of community scale, it was recommended to take the urban form feature values of compact-low rise-low network, mid compact-low rise-mid network, compact-mid rise-low network, and mid compact-mid rise-mid network types as the control threshold.

Funding

CRediT authorship contribution statement

Yunfeng Tian: Writing – review & editing, Visualization, Validation, Software, Methodology, Investigation, Formal analysis, Data curation, Conceptualization. **Shudi Zuo:** Writing – review & editing, Funding acquisition. **Jiaheng Ju:** Data curation. **Shaoqing Dai:** Formal analysis. **Yin Ren:** Supervision. **Panfeng Dou:** Formal analysis.

Declaration of competing interest

The authors declare that they have no known competing financial interests or personal relationships that could have appeared to influence the work reported in this paper.

Data availability

Data will be made available on request.

Acknowledgments

Appendix A. Supplementary data

Supplementary data to this article can be found online at https://doi.org/10.1016/j.buildenv.2023.111007.

References

[1] S. Klaric, A. Korjenic, J. Hollands, et al., Advantages of an interdisciplinary approach to the sustainable development of two scenarios in Bosnia and Herzegovina, Buildings 9 (2019) 143, https://doi.org/10.3390/buildings9060143.

[2] Center for International Knowledge on Development of China, Progress report on China's implementation of the 2030 agenda for sustainable development. http://www.cikd.org/detail?docId=1800/, 2021. (Accessed 28 May 2023).

[3] F. Creutzig, G. Baiocchi, R. Bierkandt, et al., Global typology of urban energy use and potentials for an urbanization mitigation wedge, P. Natl. Acad. Sci. USA. 112 (2015) 6283–6288, https://doi.org/10.1073/pnas.1315545112.

[4] Y. Dong, G. Jin, X. Deng, Dynamic interactive effects of urban land-use efficiency, industrial transformation, and carbon emissions, J. Clean. Prod. 270 (2020), 122547, https://doi.org/10.1016/j.jclepro.2020.122547.

[5] A. Christen, N.C. Coops, B.R. Crawford, et al., Validation of modeled carbon-dioxide emissions from an urban neighborhood with direct eddy-covariance measurements, Atmos. Environ. 45 (2011) 6057–6069, https://doi.org/10.1016/j.atmosenv.2011.07.040.

[6] S. Zuo, S. Dai, J. Ju, et al., The importance of the functional mixed entropy for the explanation of residential and transport CO_2 emissions in the urban center of China, J. Clean. Prod. 380 (2022), 134947, https://doi.org/10.1016/j.jclepro.2022.134947.

[7] K. Shi, T. Xu, Y. Li, et al., Effects of urban forms on CO_2 emissions in China from a multi-perspective analysis, J. Environ. Manag. 262 (2020), https://doi.org/10.1016/j.jenvman.2020.110300, 110300.1-110300.14.

[8] J. Ou, X. Liu, X. Li, et al., Quantifying the relationship between urban forms and carbon emissions using panel data analysis, Landsc. Ecol. 28 (2013) 1889–1907, https://doi.org/10.1007/s10980-013-9943-4.

[9] E.H. Girvetz, J.H. Thorne, A.M. Berry, et al., Integration of landscape fragmentation analysis into regional planning: a statewide multi-scale case study from California, USA, Landsc. Urban Plann. 86 (2008) 205–218, https://doi.org/10.1016/j.landurbplan.2008.02.007.

[10] C. Fan, S. Myint, A comparison of spatial autocorrelation indices and landscape metrics in measuring urban landscape fragmentation, Landsc. Urban Plann. 121 (2014) 117–128, https://doi.org/10.1016/j.landurbplan.2013.10.002.

[11] S. Lee, B. Lee, The influence of urban form on GHG emissions in the US household sector, Energy Pol. 68 (2014) 534–549, https://doi.org/10.1016/j.enpol.2014.01.024.

[12] M.W. Horner, A multi-scale analysis of urban form and commuting change in a small metropolitan area (1990–2000), Ann. Reg. Sci. 41 (2007) 315–332, https://doi.org/10.1007/s00168-006-0098-y.

[13] S. Zuo, S. Dai, Y. Ren, More fragmentized urban form more CO_2 emissions? A comprehensive relationship from the combination analysis across different scales, J. Clean. Prod. 244 (2020), 118659, https://doi.org/10.1016/j.jclepro.2019.118659.

[14] Y. Makido, S. Dhakal, Y. Yamagata, Relationship between urban form and CO_2 emissions: evidence from fifty Japanese cities, Urban Clim. 2 (2012) 55–67, https://doi.org/10.1016/j.uclim.2012.10.006.

[15] Q. Li, X. Chen, S. Jiao, et al., Can mixed land use reduce CO_2 emissions? A case study of 268 Chinese cities, Sustainability 14 (2022), 15117, https://doi.org/10.3390/su142215117.

[16] A. Sharifi, Y. Wu, D. Khamchiangta, et al., Urban carbon mapping: towards a standardized framework, Energy Proc. 152 (2018) 799–808, https://doi.org/10.1016/j.egypro.2018.09.193.

[17] H. Zhang, J. Peng, R. Wang, et al., Spatial planning factors that influence CO_2 emissions: a systematic literature review, Urban Clim. 36 (2021), 100809, https://doi.org/10.1016/j.uclim.2021.100809.

[18] Y. Wu, A. Sharifi, P. Yang, et al., Mapping building carbon emissions within local climate zones in Shanghai, Energy Proc. 152 (2018) 815–822, https://doi.org/10.1016/j.egypro.2018.09.195.

[19] D. Khamchiangta, Y. Yamagata, Mapping urban carbon emissions in relation to local climate zones: case of the building sector in Bangkok Metropolitan Administration, Thailand, Energy Built. Environ. 5 (2024) 337–347, https://doi.org/10.1016/j.enbenv.2022.11.002.

[20] M. Cai, C. Ren, Y. Shi, et al., Modeling spatiotemporal carbon emissions for two mega-urban regions in China using urban form and panel data analysis, Sci. Total Environ. 857 (2023), 159612, https://doi.org/10.1016/j.scitotenv.2022.159612.

[21] M. Cai, Y. Shi, C. Ren, et al., The need for urban form data in spatial modeling of urban carbon emissions in China: a critical review, J. Clean. Prod. 319 (2021), 128792, https://doi.org/10.1016/j.jclepro.2021.128792.

[22] J. Tan, Y. Zheng, X. Tang, et al., The urban heat island and its impact on heat waves and human health in Shanghai, Int. J. Biometeorol. 54 (2010) 75–84, https://doi.org/10.1007/s00484-009-0256-x.

[23] X. Li, P. Gong, Y. Zhou, et al., Mapping global urban boundaries from the global artificial impervious area (GAIA) data, Environ. Res. Lett. 15 (9) (2020), https://doi.org/10.1088/1748-9326/ab9be3.

[24] S.J. Davis, D. Tong, Z. Qiang, et al., Committed emissions from existing energy infrastructure jeopardize 1.5 °C climate target, Nature 572 (2019) 373–377, https://doi.org/10.1038/s41586-019-1364-3.

[25] B. Zheng, H. Huo, Q. Zhang, et al., High-resolution mapping of vehicle emissions in China in 2008, Atmos. Chem. Phys. 14 (2014) 9787–9805, https://doi.org/10.5194/acp-14-9787-2014.

[26] W. Jiang, G. He, T. Long, et al., Potentiality of using Luojia 1-01 nighttime light imagery to investigate artificial light pollution, Sensors 18 (2018) 2900, https://doi.org/10.3390/s18092900.

[27] X. Zhang, L. Liu, X. Chen, et al., GLC_FCS30: global land cover product with fine classification system at 30 m using time-series Landsat imagery, Earth Syst. Sci. Data 13 (2021) 2753–2776, https://doi.org/10.5194/essd-13-2753-2021.

[28] P. Gong, B. Chen, X. Li, et al., Mapping essential urban land use categories in China (EULUC-China): preliminary results for 2018, Sci. Bull. 65 (2020) 182–187, https://doi.org/10.1016/j.scib.2019.12.007.

[29] V. Modrak, Z. Soltysova, Development of operational complexity measure for selection of optimal layout design alternative, Int. J. Prod. Res. 56 (2018) 7280–7295, https://doi.org/10.1080/00207543.2018.1456696.

[30] W. Liao, T. Hong, Y. Heo, The effect of spatial heterogeneity in urban morphology on surface urban heat islands, Energy Build. 244 (2021), 111027, https://doi.org/10.1016/j.enbuild.2021.111027.

[31] C. Yin, M. Yuan, Y. Lu, et al., Effects of urban form on the urban heat island effect based on spatial regression model, Sci. Total Environ. 634 (2018) 696–704, https://doi.org/10.1016/j.scitotenv.2018.03.350.

[32] W. Quan, N. Jian, J. Tenhunen, Application of a geographically-weighted regression analysis to estimate net primary production of Chinese forest ecosystems, Global Ecol. Biogeogr. 14 (2010) 379–393, https://doi.org/10.1111/j.1466-822X.2005.00153.x.

[33] M. Cahill, G. Mulligan, Using geographically weighted regression to explore local crime patterns, Soc. Sci. Comput. Rev. 25 (2007) 174–193, https://doi.org/10.1177/0894439307298925.

[34] M. Hu, Z. Li, J. Wang, et al., Determinants of the incidence of hand, foot and mouth disease in China using geographically weighted regression models, PLoS One 7 (2012), e38978, https://doi.org/10.1371/journal.pone.0038978.

[35] X. Hu, L.A. Waller, M.Z. Al-Hamdan, et al., Estimating ground-level PM2. 5 concentrations in the southeastern US using geographically weighted regression, Environ. Res. 121 (2013) 1–10, https://doi.org/10.1016/j.envres.2012.11.003.

[36] R.H. Lyles, Regression methods in biostatistics: linear, logistic, survival, and repeated measures models, J. Am. Stat. Assoc. (2006), https://doi.org/10.1007/978-1-4614-1353-0.

[37] F. Yao, H. Zhu, M. Wang, The impact of multiple dimensions of urbanization on CO_2 emissions: a spatial and threshold analysis of panel data on China's prefecture-

level cities, Sustain. Cities Soc. 73 (2021), 103113, https://doi.org/10.1016/j.scs.2021.103113.

[38] T.M. Khanna, G. Baiocchi, M. Callaghan, et al., A multi-country meta-analysis on the role of behavioural change in reducing energy consumption and CO_2 emissions in residential buildings, Nat. Energy 6 (2021) 925–932, https://doi.org/10.1038/s41560-021-00866-x.

[39] M. Wang, H. Xu, The impact of building height on urban thermal environment in summer: a case study of Chinese megacities, PLoS One 16 (2021), e0247786, https://doi.org/10.1371/journal.pone.0247786.

[40] S.Y. Chan, C.K. Chau, On the study of the effects of microclimate and park and surrounding building configuration on thermal comfort in urban parks, Sustain. Cities Soc. 64 (2021), 102512, https://doi.org/10.1016/j.scs.2020.102512.

[41] S. Yang, L.L. Wang, T. Stathopoulos, et al., Urban microclimate and its impact on built environment–A review, Build. Environ. 238 (2023), 110334, https://doi.org/10.1016/j.buildenv.2023.110334.

[42] L. Martinelli, A. Matzarakis, Influence of height/width proportions on the thermal comfort of courtyard typology for Italian climate zones, Sustain. Cities Soc. 29 (2016) 97–106, https://doi.org/10.1016/j.scs.2016.12.004.

[43] X. Li, Research on the Characteristics of Living Carbon Emissions of Residents in High-Density Residential Communities in Beijing, North China University of Technology, 2022, https://doi.org/10.26926/d.cnki.gbfgu.2022.000282.

[44] P.L. Mokhtarian, X. Cao, Examining the impacts of residential self-selection on travel behavior: a focus on methodologies, Transport. Res. B-Meth. 42 (2008) 204–228, https://doi.org/10.1016/j.trb.2007.07.006.

[45] C.R. Bhat, N. Eluru, A copula-based approach to accommodate residential self-selection effects in travel behavior modeling, Transport. Res. B-Meth. 43 (2009) 749–765, https://doi.org/10.1016/j.trb.2009.02.001.

[46] J. Wang, T. Zhang, B. Fu, A measure of spatial stratified heterogeneity, Ecol. Indicat. 67 (2016) 250–256, https://doi.org/10.1016/j.ecolind.2016.02.052.

[47] J. Wang, C. Jiang, L. Li, et al., Spatial Sampling and Statistical Inference, Science Press, 2009.

[48] A.Z. Tugrul, Urban energy modelling approaches: a literature review, Int.J. Energy Smart Grid 5 (2020) 57–64, https://doi.org/10.23884/IJESG.2019.4.2.02.

[49] C.D. Elvidge, K. Baugh, M. Zhizhin, et al., VIIRS night-time lights, Int. J. Rem. Sens. 38 (2017) 5860–5879, https://doi.org/10.1080/01431161.2017.1342050.

[50] W. Wang, C. Cao, Y. Bai, et al., Assessment of the NOAA S-NPP VIIRS geolocation reprocessing improvements, Rem. Sens. 9 (2017) 974, https://doi.org/10.3390/rs9100974.